On the Role of Modeling Dust Production by Fragmenting Warheads in Storage Facilities

Dr. Joseph D. Baum; Applied Simulations, Inc.; 1210 Pine Hill Road;
McLean, VA 22101, USA.

Dr. Orlando Soto; Applied Simulations, Inc.; 1210 Pine Hill Road
McLean, VA 22101, USA.

Dr. Fumiya Togashi; Applied Simulations, Inc.; 1210 Pine Hill Road,
McLean, VA 22101, USA.

Prof. Rainald Löhner; George Mason University; Fairfax, VA 22030, USA.

Mr. Robert A. Frank; Applied Research Associates Inc.; 8537 Six Forks Rd, Suite 600,
Raleigh, NC 27615, USA.

Dr. Ali Amini; Defence Threat Reduction Agency; 8725 John J. Kingman Rd,
Fort Belvoir, VA 22060, USA.

KEYWORDS

CFD, CSD, airblast, breach, blast propagation, dust, cased munitions.

ABSTRACT

The paper presents the results of a coupled Computational Fluid Dynamics (CFD)/Coupled Structural Dynamics (CSD) simulations of cased charges internal detonation within reinforced concrete chambers; a part of a test and modeling effort studying air blast propagation through breached walls.

Initial simulations calibrated the CFD/CSD model and determined the physical mechanisms controlling internal blast environments, wall breach, and blast propagation through the breach. In the test, the detonation room (composed of two test walls and two culverts) incurred significant damage due to the fragments and blast loads. Both culverts failed. Initial coupled CFD/CSD simulations modeled the culverts as non-responding surfaces. These simulations reproduced the damage to the test walls, but the pressure histories matched the experimental data **only** out to ~10 ms. Subsequent airblast reflections were significantly reduced. Post-test damage analysis showed significant fragment damage to the culverts, with the concrete stripped to the first layer of rebars. Repeat simulations, where the culvert response, dust production and dust absorption of kinetic and thermal energy were modeled, matched the experimental data.

Additional simulations provided a synthetic database for fast running model development (FRM). These includes modeling of breaching (size and timing), secondary debris, and blast propagation through the breach opening.

INTRODUCTION

The simulations presented here are part of a test, analysis, and modeling effort investigating airblast propagation through breached walls. The coupled CFD/CSD simulations are providing additional insight and details not measured in the tests, as well as developing a synthetic database to supplement the test matrix.

The numerical simulation of blast waves and fragment propagation through failing walls involves several physical processes as well as several coupled numerical schemes. The controlling physical mechanisms include: detonation wave initiation, detonation wave propagation through the explosive, charge case expansion under the extreme load, case cracking, break-up and formation of fragments, detonation products expansion through the forming cracks, and detonation products and case fragments impact on the facility walls, wall response and failure, and blast wave as well as secondary debris (ejecta, dust, rebars and other first wall debris) impact on the next-layer of walls, and their response.

Modeling of the many interactive physical processes requires coupling of several methodologies, describing both the fluid dynamic and structural dynamics processes. Over the last several years we have developed a numerical methodology that couples state-of-the-art Computational Fluid Dynamics (CFD) and Computational Structural Dynamics (CSD) methodologies. The flow code solves the time-dependent, compressible Euler and Reynolds-Averaged Navier-Stokes equations on an unstructured mesh of tetrahedral elements. The CSD code solves explicitly the large deformation, large strain formulation equations on an unstructured grid composed of bricks and hexahedral elements. The codes are coupled via a 'loose coupling' approach which decouples the CFD and CSD sets of equations and uses projection methods to transfer interface information between the CFD and CSD domains. The coupling modularity is kept by the addition of a `controller' code, which handles the transfer of information between the different solvers, non-matching meshes at the interface and incorporates conservative interpolation schemes and fast techniques for neighbor search.

TEST SETUP

Figure 1 shows the test configuration. The test structure consisted of a disposable burst room composed of two culvert sections. A reuseable thick reinforced concrete closure panel with a doorway is placed at the far end to provide confinement and controlled venting of the structure. The permanment portion of the test structure is designed to study the failure of the first wall, propagation of blast and debris into the second bay, and progressive loading and failure of the second wall. The facility incorporates two replaceable test walls, loaded with load beams to ensure full enclosure during the test. The replaceable test walls permit us to quickly reconstruct the test facility and study the effect of wall geometry, reinforcing, and material strength as well as weapon size and standoff.

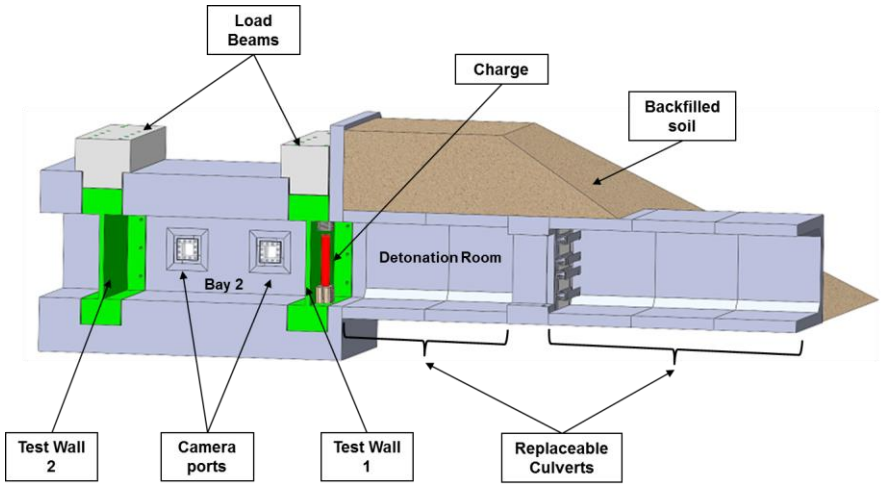

Figure 1. Test Configuration

Figure 2 shows the instrumentation for the test. Instrumentation in the burst room consisted of four pressure gages on the ceiling of the culvert sections. Six additional pressure gages were placed in Bay 2, four on the ceiling and two on the front face of the second test wall. Accelerometers, three on both test walls, provided a measure of the structural response of the two walls. Two camera ports in Bay 2 provided high speed video of the failure and debris ejection off of wall 1. Two exterior cameras provided high speed video of the wall 2 response.

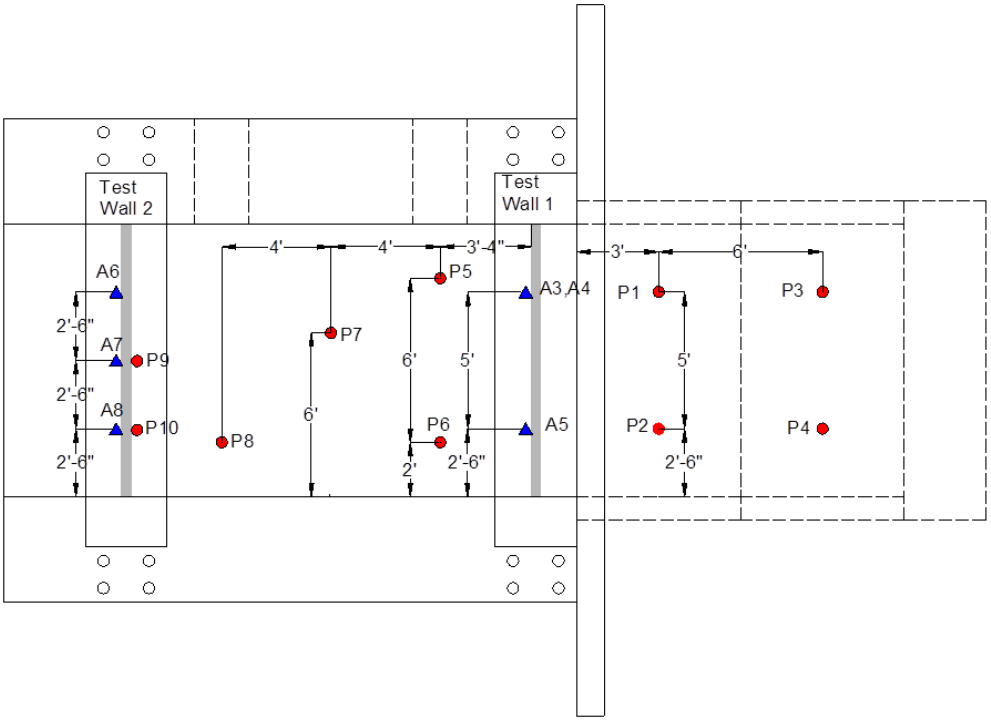

Figure 2. Instrumentation Layout (top view)

FEMAP SIMULATION

CSD/CFD Code Description

Any blast-structure simulation proceeds through the following stages: 1. Pre-Processing; 2. Grid Generation; 3. Coupled Fluid/Structure Solver; and 4. Post-Processing

Automatic unstructured mesh surface and volume generation has reached a high level of maturity over the past several years. The graphic pre-processor FECAD (Löhner 2001) enables the preparation of the data sets for the solver and the mesh generator FRGEN3D. It also quickly generates CSM meshes from existing CFD domains, thereby easing the process of setting up a complex-geometry coupled problem (Baum 2004, Baum 2008).

Mesh generation for both the CSM and CFD is performed using FRGEN3D (Löhner 1988, 1996). This unstructured grid generator is based on the advancing front method. The CFD mesh is composed of triangular (surface) and tetrahedral (volume) elements. The CSM mesh includes beams, triangular or quad shells and bricks or hexahedra (solids). Although the angles of a typical hex are less than perfect, extensive testing against perfect-angle bricks for both linear and nonlinear cases produced almost identical results. This, nevertheless, necessitated the replacement of the Belytschko-Tsay hourglass control model (default model in DYNA3D (Whirley 1991), with the Flanagan-Belytschko hourglass control model (model no. 3 in DYNA3D), incurring a 30% performance penalty.

The flow solver employed is FEFLO, a 3-D adaptive, unstructured, edge-based hydro-solver based on the Finite-Element Method Flux-Corrected Transport (FEM-FCT) (Löhner 1992). It solves the Arbitrary Lagrangean-Eulerian (ALE) formulation of the Euler and Reynolds-averaged turbulent, Navier-Stokes equations. In addition to the more mature, FEM-FCT, several shock capturing features have been added over the years: Rieman solvers with a choice of limiters, Roe solvers [Löhner 2008], high-order (to eight) ENO schemes (Luo 2007), and the latest Discontinuous Galerkin solvers (Luo 2011). The spatial mesh adaptation is based on local H-refinement, where the refinement/deletion criterion is a modified H2-seminorm (Löhner 1992) based on user-specified unknowns. Equations of state (EOS) supported by FEFLO include ideal polytropic gas, real air EOS table look-up, water EOS table look-up, a link to the SESAME library of EOS, and the JWL EOS and several afterburning and combustion models (Togashi 2006, Togashi 2011). Flows with particles are treated via a second solid phase. The particles interact with the fluid, exchanging mass, momentum and energy, and are integrated in a time-

consistent manner with the fluid. Flows with multiple moving bodies are handled using an embedded approach (Löhner 2004).

The CSD code is ASICSD, a new CSD code intended to model large structural deformations (Soto 2005, Soto 2007, Soto 2010). This is an unstructured, explicit finite element code, well suited for modeling large deformations. It provides a good base for non-linear materials with elasto-plastic compartmental laws with rupture. The code incorporates a large library of materials and various equations-of-state, as well as many kinematic options, such as slidelines and contacts. ASICSD models the weapon detonation/fragmentation, as it can model case cracking (thermal softening was defined by the Johnson and Cook model [Johnson 1983]). ASICSD solves the continuous mechanics equilibrium equation. The weak formulation (virtual work principle) is written in the spatial configuration (actual configuration) and it is discretized in time using an explicit second-order central difference scheme. In space, the virtual work equation is solved by using stable finite element types. The most commonly used elements are: a fully integrated large-deformation Q1/P0 solid element (hexahedra with an 8 nodes interpolation scheme for the kinematic variables and constant pressure) which does not present hourglass modes and does not lock for incompressible cases. Several 3-node and 4-node large-deformation shell elements (Hughes-Liu shell, Belytschko shells, MITC shells, ASGS stabilized shells) which are formulated using standard objective stress update schemes (Jaumann-Zaremba, co-rotational embedded axis, etc,), are fully integrated to avoid hourglass spurious modes. Finally, some objective truss and beam elements (i.e. Belytschko and Hughes-Liu beams) have also been implemented. Many different material models have been included into the code. The most commonly used are: a plasticity model which relies on a hyper-elastic characterization of the elastic material response for the solid elements, and a standard hypo-elastic plasticity model for the shell, beam and truss elements. The most often used failure criterion is based on the maximum effective plastic strain and the stress tensor inside the element. The fracture may be simulated by element erosion and/or node disconnection. The code is fully parallelized using both OpenMP and MPI directives. The code has been extensively validated (Soto 2005, Soto 2007, Soto 2010).

Coupling between all modules is provided by FEMAP, via a loose-coupling approach. The embedded approach is used to couple the CFD and CSM module (Löhner 2007).

Simulation Model Details

Figure 3 shows some of the CSD modeling details of the facility, test walls, and explosive case. The modeled facility included two rooms, the detonation room and bay room. In the initial simulation, each room's ceiling, floor and culverts were modeled as non-responding. Only the two test walls were allowed to respond. The test walls were modeled with 0.5 inch solid elements with beams used to model the rebar.

The weapon case was modeled with 0.1 inch size elements. The Tritonal and C4 booster explosives were both modeled with a JWL equation-of-state. Past attempts to model Tritonal using simple JWL equation-of-state were not successful. However, the latest chemical kinetics models incorporated within FEFLO resulted in blast wave evolution that was in excellent agreement with the data, as will be shown later.

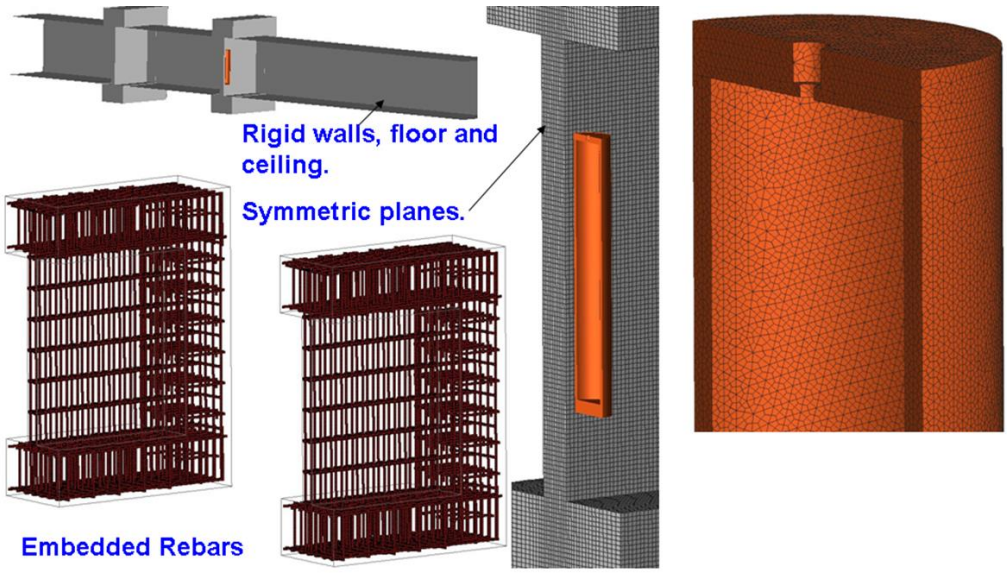

Figure 3. CSD/CFD Modeling details of the Test Facility, Explosive Charge, and Test Walls

RESULTS AND DISCUSSIONS

Figure 4 shows the damage to the two test walls post-test. Both walls were catastrophically destroyed. High speed video (Figure 5a) shows that test wall 1 initially breached over the middle third of the wall, propagating blast pressure and high speed debris into the second bay. The FEMAP simulation replicates this initial breach, as shown in Figure 5b. The simulation also agreed reasonably well on the maximum debris velocity measured from the video.

Later time pressures were sufficient to fail and remove both the wing walls. Note the large chunks of debris that remained entangled in the rebar and on the floor over the front third of bay 2. The combined pressure and debris loading on test wall 2 was sufficient to fail test wall 2 which sheared at the top and rotated downward, as shown in Figure 4b.

a. Internal view of test wall 1 b. External view of test wall 2

Figure 4. Post-test photographs of test walls

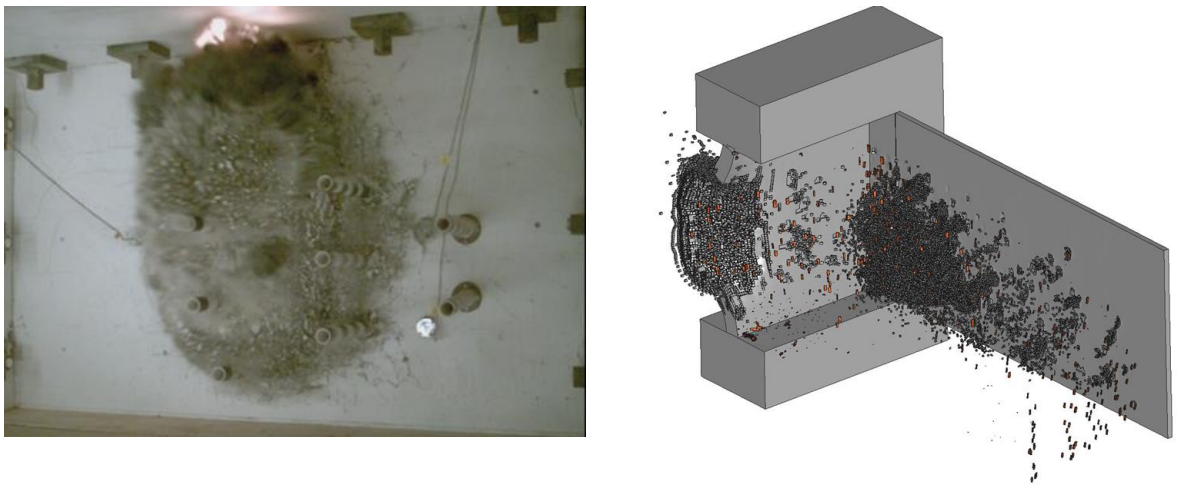

a. High speed video clip b. FEMAP simulation

Figure 5. Initial breach of test wall 1

Figure 6 shows a sequence of snapshots taken at three times during the detonation process: at the middle of the detonation, at the end and sometime afterwards. In each panel shown are the velocity contours on the plane-of-symmetry (left), the pressure on the structure (center) and the velocity of all structural elements (right). The figures exhibit: 1) the top, point detonation initiation and propagation down the explosive; 2) the case expansion and break-up (initial case failure is at the weld between the base plate and the cylindrical charge, failing due to shear); 3) detonation products escape through the expanding cracks (notice that due to the large pressure ratio, the detonation products achieve supersonic speeds upon expansion, cooling down and thus strongly affecting the later combustion of any aluminized particles or other additives); 4) the high speed cylindrical fragment expansion and the low velocity base and tail plates fragments; and 5) wall breach. While a significant pressure load is imposed on the wall, the initial breach resulted from fragment loading, which was significantly higher than pressure loading at this time.

Figure 7 shows test walls response at 5.0, 10.0 and 20.0 ms. Shown at each time are the structural surface, including the secondary debris and the breaking rebars, the structural component velocity, and the damage contour plots (where zero is non-damaged, and 2.0 is totally-damaged., i.e., the deviatoric stresses are zero, and the element can only withstand compression, but not tension or shear). The blast wave propagating through the breach has arrived to test wall 2 well before the slower-propagating secondary debris. Still, the airblast pressure loading was not sufficient to fail the wall: a large debris loading from the first wall failure contributed substantially to the failure of the second wall as observed in the test.

Comparison of pressure time histories at three locations is shown in Figure 8. Figure 8a shows comparison for a station in the blast room, while Figure 8b and Figure 8c show comparisons for stations in the bay area. In the blast room, the results show excellent agreement between the measured and predicted data in terms of shock arrival time, the ceiling-reflected shock and side-wall reflected shock. Until 10 ms, all shock reverberation features are captured correctly. However, at 10 ms the simulations predict the arrival of the reflected shock from the back side of the room, opposite test wall 1, while the test results do not show this reflection. Similarly, the predictions in the bay room track the experimental data nicely until 11ms, and then deviate drastically.

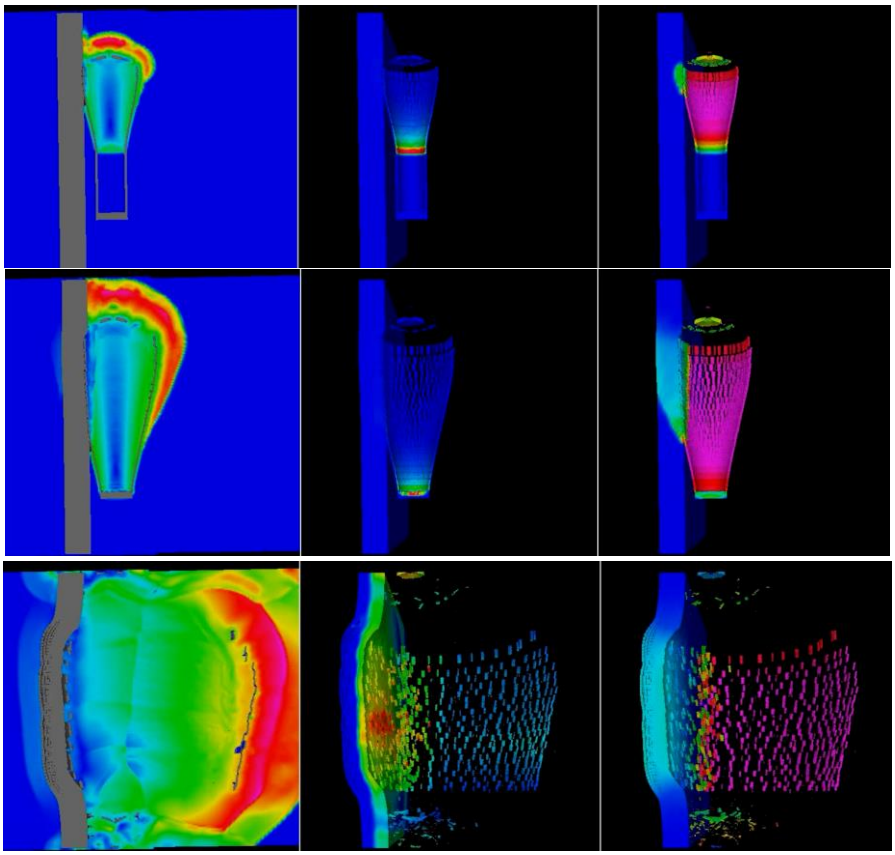

Figure 6. Detonation, case fragmentation and wall breach. Shown are the fluid velocity contours, and the resulting structural pressure and velocity at 3 times during detonation and wall breach

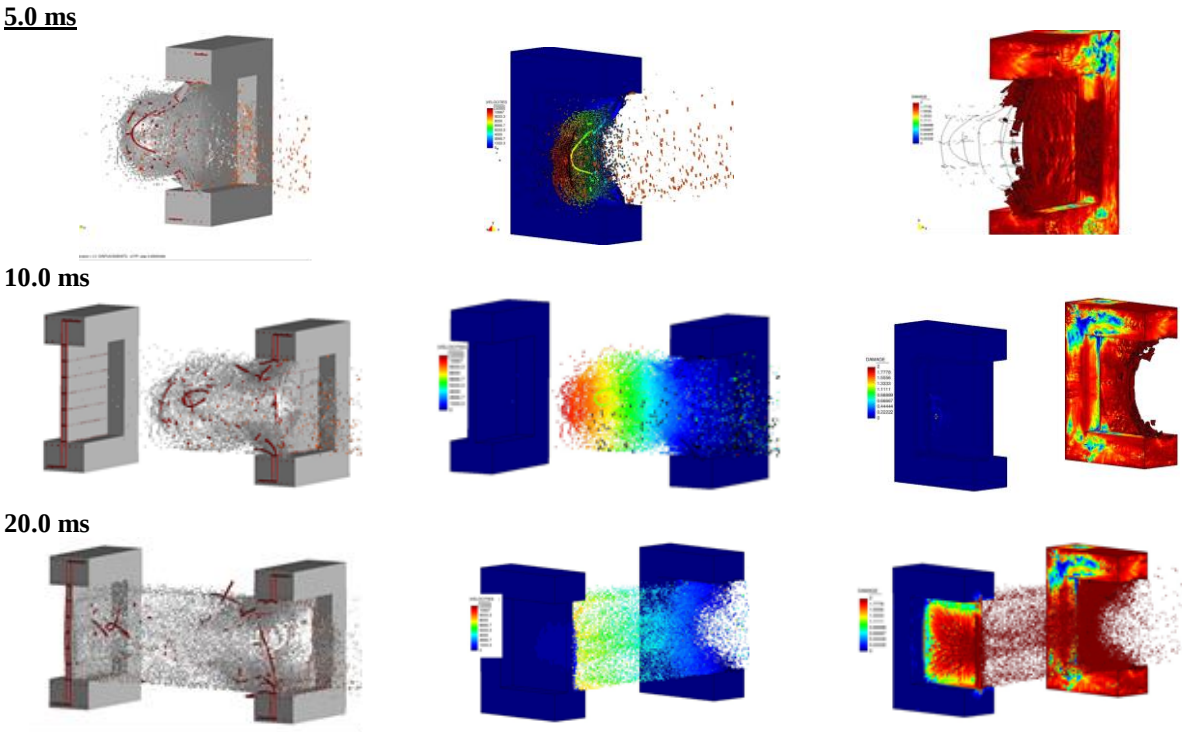

Figure 7. Test walls response at 5.0, 10.0 and 20.0 ms. Shown are the CSD surfaces, including secondary debris and fragments, CSD velocity and test wall damage contours

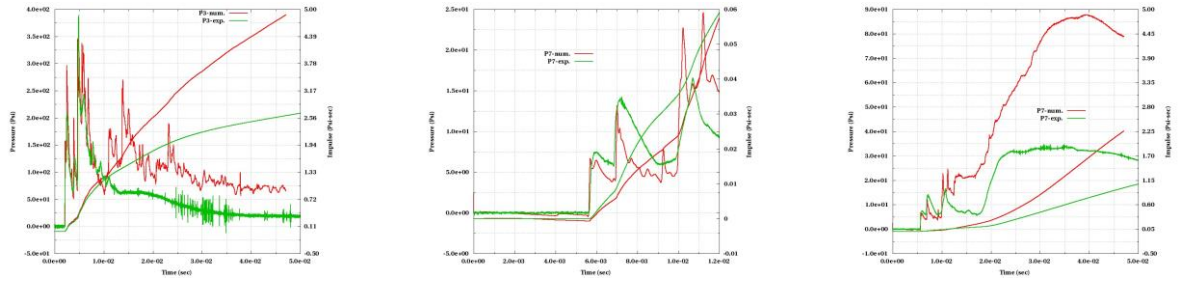

a. Detonation room b. Bay 2 P7 early time c. Bay 2 longer time frame

Figure 8. Comparison of measured and predicted pressure time histories at three locations, one in the detonation room and two in the Bay room

A careful analysis of post-test results helped explain this phenomenon. The culvert post-test shots (Figure 9) indicate that weapon fragment impacts on the side culverts resulted in complete stripping of the concrete cover to the first rebar cage. We estimated the amount of concrete stripped at several hundred kilograms. This clearly indicated that modeling of the culvert as non-responding was not appropriate. Hence, we repeated the simulation this time modeling the culvert as any other reinforced concrete wall, including concrete failure and pulverization in response to the high-speed weapon fragments impact.

Figure 10 shows the CSD surfaces and damage contours at 1.5 ms and 3.0 ms. At this early time the breach damage to the test is identical to the breach damaged obtained in the no-dust previous simulation. In addition, significant damage is now observed along the culvert side walls, due to high-speed fragment impact. The model predicted stripping of the concrete to the first layer of rebars, in agreement with the observed test results.

Figure 11 show the time evolution of dust mass injection into the room and the injection velocity. Most dust is injected within the first 6.0 ms. Since the detonation room is fairly long, there is a time span between the fragment impact near the test wall to fragment impact on the culvert at the far end of the room. The fragments impact the wall at velocities of about 1.0 km/sec, and the dust is blown off the wall with initial velocities of 300 to 600 m/s. The dust velocity decays rapidly after ejection, as the dust blown off the wall encounters the high pressure blast wave, which at these ranges, lags the case fragments.

Figure 9. Test results show the significantly damaged east and west culverts

1.5 ms

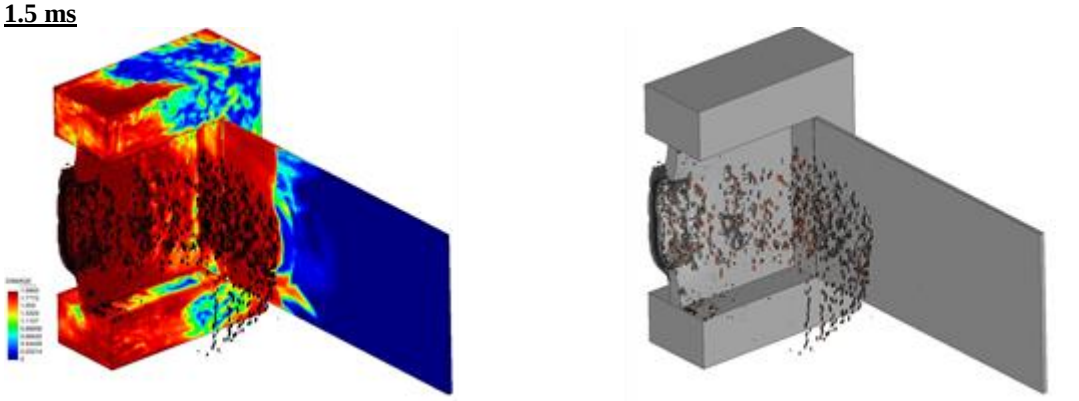

3.0 ms

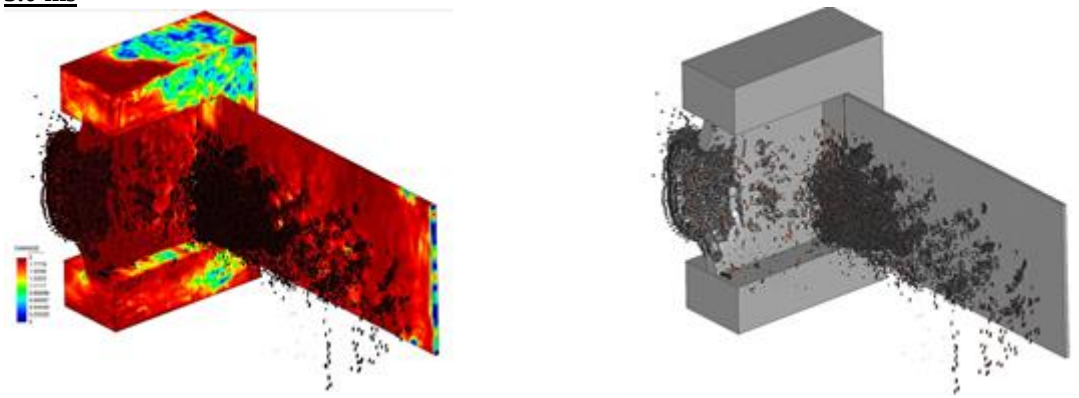

Figure 10. CSD surfaces and damage contours at 1.5 and 3.0ms

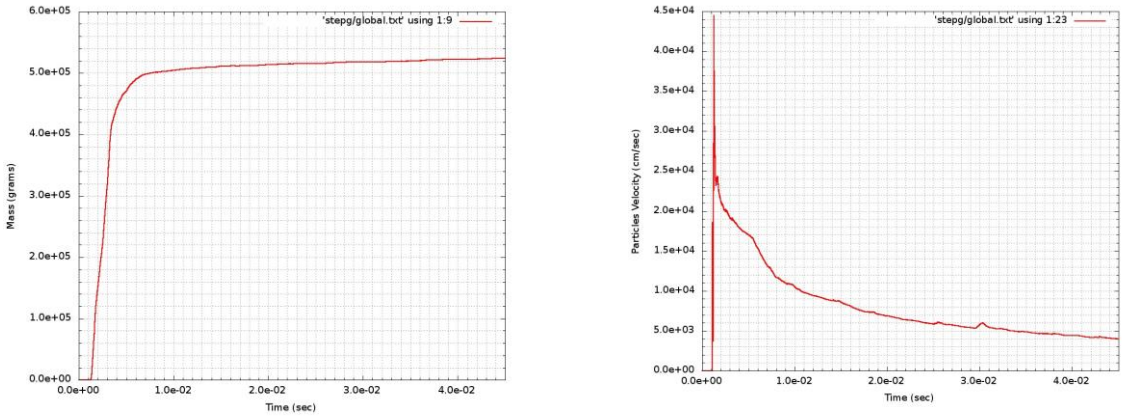

Figure 11. Temporal evolution of dust mass injection and dust velocity off the culvert walls

Finally, we compare predicted and measured pressure and impulse time histories at several locations, as well as measured and predicted walls response (acceleration and deflection) for the two test walls, obtained when incorporating dust production from the culverts in the simulation. Figure 12a shows a comparison for stations 1 and 2 (symmetric) in the detonation room. The experimental data is in black, the previous no-dust prediction is in green, and the new predicted results modeling dust is in red. The difference between the predictions is strikingly evident at about 10 ms, when the reflected shock from the room far end attempts to propagate towards the test walls. The reflected wave now encounters several hundred kilograms of fine dust. The reflected wave is now damped (i.e., significant energy loss) due to: 1) thermal (internal) energy loss as the dust particles internal energy increases due to heating by the hot detonation products; and 2) drag damping (kinetic energy loss), as the blast wave accelerates the slower particles.

The corrected description of the controlling physical processes (i.e., dust losses) yields a more accurate blast wave energy damping, as shown in Fig 12a for a station in the blast room. Similar results were obtained for two stations in the bay room: station 8 located on the ceiling, and station 10, located on test wall 2 (Figs 12b and 12c, respectively). Finally, the more accurate pressure environment prediction resulted in a more accurate structural response prediction. Figures 13a and 13b show comparisons of measured and predicted accelerations and displacements for test walls 1 and 2, respectively. Very good agreement is demonstrated both in terms of acceleration and displacement.

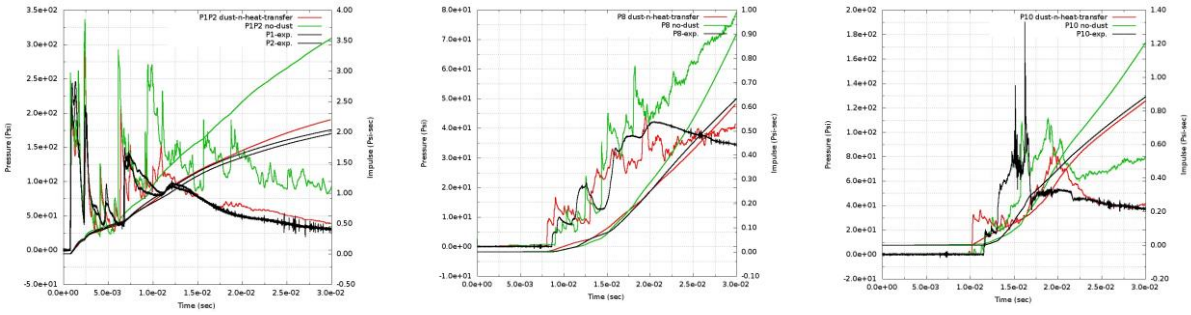

a. Burst room b. Bay 2 on ceiling c. Bay 2 On test wall 2

Figure 12. Comparison of measured and prediction results for pressure

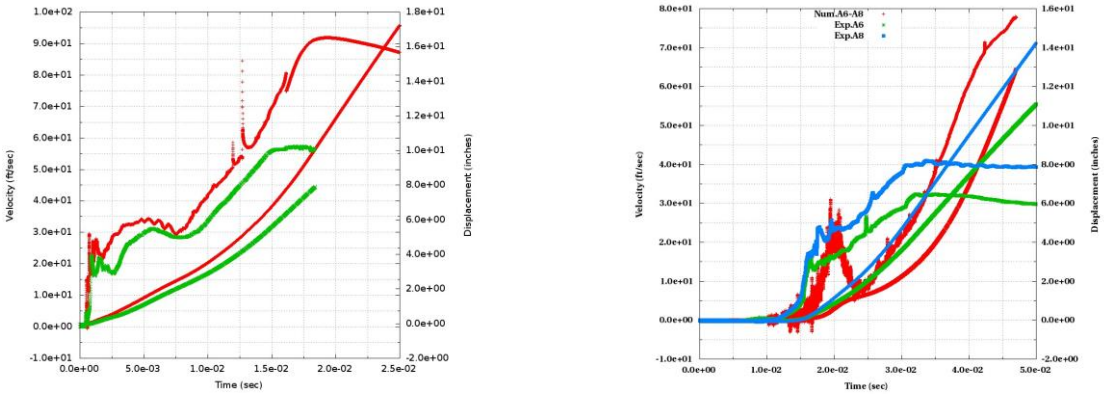

a. Test wall 1 b. Test wall 2

Figure 13. Comparison of measured and predicted wall motions

FUTURE PLANS

In all, 12 tests were conducted varying wall thickness, weapon standoff, and concrete material type (conventional and high strength concrete). Additional tests are being simulated to further validate the FEMAP simulation model. Once a validated model has been confirmed, the coupled CSD/CFD model will be used to develop a synthetic database for engineering model development. The test simulations are also providing valuable insight into the blast propagation through the wall breach.

CONCLUSIONS

The simulations presented in this paper are part of a test, analysis, and modelling effort studying air blast propagation through breached walls. FEMAP, a coupled CFD/CSD methodology was used to model internal detonations of cased munitions against reinforced concrete walls.

Initial simulations were performed to determine the controlling physical mechanisms controlling the internal environments, wall breach and blast propagation through the failing walls. The initial simulation modelled the response of two reinforced concrete walls to loads from a cased charge placed in close proximity to the center of wall 1. In the test, the detonation room (composed of two culverts) incurred significant damage due to fragments and blast load. Test wall 1 was initially breached over the middle third, with the wing walls removed by the later time blast loads. Debris from test wall 1 impacted wall 2 that failed under the combined blast and debris loads.

The first simulation modelled test wall response, but modelled the culverts as rigid, non-responding surfaces. These simulations reproduced the damage to the test walls, but the pressure histories matched the experimental data only out to about 10 ms. Further analysis of the test results indicated large damage to the culverts and significant dust production by the failing concrete. A repeat simulation where the culvert response was modelled and the dust was allowed to absorb both kinetic and thermal energy, matched the experimental data significantly better.

ACKNOWLEDGMENTS

The authors gratefully acknowledge the financial support provided by the Defense Threat Reduction Agency, DTRA/J9CXSS and DTRA/J9CXT. Mr. Michael. E. Giltrud and Ms. Audrey Kersul serve at the Technical Control Monitors.

REFERENCES

Baum, J.D., Mestreau, E., Luo, H., Löhner, R., Pelessone, D., Charman, C., (2004) "Recent Development of a Coupled CFD/CSD Methodology Using an Embedded Approach." Proc. 24th Inter. Shock wave Symposium, Beijing, China, July.

Baum, J.D., Mestreau, E., Löhner, R. & Charman, C., (2007) "An Experimental and Numerical study of Steel Tower Response to Blast Loading", Proc. of the 26th International Symposium on Shock Waves, Göttingen, Germany, July 15-20.

Baum, J.D., Soto, O.A., Charman, C., Mestreau, Löhner, R., and Hastie, R. (2008) "Coupled CFD/CSD Modelling of Weapon detonation and Fragmentation, and Structural Response to the Resulting Blast and Fragment Loading," NDIA Warhead ballistic conference, Feb 2008, Monterey, CA.

Löhner, R. and P. Parikh, P. (1988), "Three-Dimensional Grid Generation by the Advancing Front Method" Int. J. Num. Meth. Fluids 8. 1135-1149.

Löhner, R. and Baum, J.D. (1992), "Adaptive H-Refinement on 3-D Unstructured Grids for Transient Problems; Int. J. Num. Meth. Fluids 14, 1407-1419.

Löhner, R. (1996) "Extensions and Improvements of the Advancing Front Grid Generation Technique," Comm. Num. Meth. Eng. 12, 683-702.

Löhner, R., Yang, C., Cebral, J.R. Soto, O.A., Camelli, F., Baum, J.D., Luo, H., Mestreau, E., and Sharov (2001) "Advances in FEFLO"; AIAA-01-0592.

Löhner, R., Baum, J.D., Mestreau, E., Sharov, D., and Charman, C. (2004) "Adaptive Embedded Unstructured Grid Methods," Int. J. Num. Meth. Eng., 60, 641-660.

Löhner, R., Cebral, J.R., Camelli, F.F., Baum, J.D., and Mestreau, E.L, and Soto, O.A. (2007) "Adaptive Embedded/Immersed Unstructured Grid Techniques," Arch. Comp. Meth. Eng. 14, 279-301.

Luo, H., Baum, J.D., and Löhner, R. (2007) "A Hermite WENO-Based Limiter for DG Methods on Unstructured Grids.; AIAA-07-0510.

Luo, H., Baum, J.D. and Löhner, R. (2011) "A Discontinuous Galerkin Method Based on a Taylor Basis for the Compressible Flows on Arbitrary Grids." AIAA-07-4080-CP.

Soto, O.A., Baum, J.,D., Löhner, R., Mestreau, E. Luo, H., (2005), "A CSD Finite Element Scheme for Coupled Fluid-Solid Problems". Fluid Structure Interaction 2005. September 19-21. La Coruna, Spain.

Soto, O.A., Baum, J.D., Mestreau, E., and Löhner, R., (2007) "An Efficient CSD FE Scheme for Coupled Blast Simulations". Ninth US National Congress on Computational Mechanics, San Francisco, CA, July 22-26.

Soto, O.A., Baum, J.D., and Löhner, R, (2010) "An efficient fluid-solid coupled finite element scheme for weapon fragmentation simulations. Eng. Fracture Mech.", Vol 77, 549-564.

Togashi, F., Löhner, R. and Tsuboi, N. (2006) "Numerical Simulation of H2/Air Detonation Using Detailed Reaction Models", AIAA-06-0954.

Togashi, F., Baum, J.D., and Löhner, R., (2011) "Numerical Modeling of Aluminum Burning for Heavily Aluminized HE" AIAA-11-3588.

Whirley, R.G. Whirley and Hallquist, J.O. (1991), “DYNA3D, A Nonlinear Explicit, Three-Dimensional Finite Element Code for Solid and Structural Mechanics”, User Manual; UCRL-MA-107254, also Comp. Meth. Appl. Mech. Eng. 33, 725-757 (1982).

.